Determination of Electron Density Profiles and Area from Simulations of Undulating Membranes
Supporting Material

Anthony R. Braun[1], Erik G. Brandt[2], Olle Edholm[2],
John F. Nagle[3] and Jonathan N. Sachs[1,*],

[1] *Department of Biomedical Engineering,*
University of Minnesota
Minneapolis, MN, USA

[2] *Department of Theoretical Physics,*
Royal Institute of Technology (KTH),
Stockholm, Sweden

[3] *Carnegie Mellon University,*
Pittsburgh, PA, USA

March 15, 2011

*Corresponding author. Electronic address: jnsachs@umn.edu.

Contents

I. Simulation details

The atomic coordinates of crystalline 1,2-dimyristoyl-sn-glycero-3- phosphocholine [DMPC] (1) was used as a scaffold for all lipid bilayer structures. This unit cell was replicated to the desired number of lipids (32–1024) and rescaled in agreement with the area per lipid $a = 0.606$ nm^2 determined in experiments (2). After hydration by 23 waters per lipid, the bilayers were simulated for 500 ns in order to allow for equilibration and development of undulations. The lipids were modeled by the force field of Berger and coworkers (3) [atomistic but with nonpolar hydrogens included into particle beads for the CH, CH_2 and CH_3 groups], while the SPC model (4) was used for the water molecules. The equations of motion were integrated using a leap-frog algorithm as implemented in the GROMACS 4 molecular dynamics program (5). The simulations were run in the isothermal-isobaric (NPT) ensemble at constant temperature and pressure, corresponding to 300 K and 1 bar, respectively.

The integration was done with constrained bond lengths and time step of 4 fs. A neighbor list was used up to 1.0 nm and updated every 10:th step. Van der Waals interactions were truncated at 1.0 nm, but the electrostatic interactions were calculated with the Particle Mesh Ewald [PME] (6, 7) algorithm beyond this distance (with grid spacing 0.12 nm). The temperature and pressure were controlled with the Nose-Hoover (8, 9) thermostat and Parrinello-Rahman (10, 11) barostat, respectively. The time constants were 1.0 ps for the thermostat and 10.0 ps for the barostat. The lateral (x, y) and normal (z) dimensions of the simulation box were coupled to independent barostats to give a tensionless bilayer.

II. The Hamming filter

This section reports Undulation Reference Surfaces (URS) and Electron Density Profiles (EDP) calculated with the Hamming Finite Response (FIR) filter (12). This filter is usually employed in signal processing applications to avoid spurious presence of ringing in the Fourier signal, which is induced by the sharp large-q cutoff of the ID filter. The extent of the ringing can be determined by comparing the one-dimensional spectrum generated by taking both the inverse and forward two-dimensional Fourier transform of the filtered undulation spectrum. If the small q mode distortion, or the intensity of the large-q ringing, perturbs the one-dimensional spectrum away from the q^{-4} undulation regime, use of a FIR filter will dampen these artifacts.

In the present study, ringing artifacts are minor due to that the intensities of the large-q modes are fairly small. Table S1 compares the percentage change of the root mean square difference (RMSD) when the URS is calculated with the Hamming filter instead of the Ideal (ID) or L4 filters [Table 2 in the main text (13)]. Fig. S1 illustrates that filtered one-dimensional spectrum fall between the linear q^{-4} dependence of the L4 filter and the sharp truncation of the ID filter. The URS calculated with the FIR filter (Fig. S2) are in good agreement to URS calculated with the ID and L4 filters, for both the Direct Fourier (DF) and Real-space Interpolation (RI) methods regardless of whether terminal carbon (TC) or phosphorus (P) atoms are selected (Fig. 3 of the main text (13) and Fig. S3, respectively). Fig. S4 presents the EDP (A) and RMSD plots (B and C) for the Hamming filter, showing very similar trends as the ID filter results [Fig. 6 of the main text (13)]. Fig. S5 compares the excess area per lipid, $\langle \Delta A_L \rangle$, calculated along the undulation surface with the Hamming filter. The result for $\langle \Delta a_L \rangle$ is slightly larger compared to the result for the ID filter (Fig. S12).

Table S1: Percentage difference in excess area per lipid $\langle \Delta a_L \rangle$ from method a1 and a2 using the Hamming filter compared to the Ideal (ID) filter.

Method	$\langle \Delta a_L^{(1)} \rangle$	$\langle \Delta a_L^{(2)} \rangle$
DF:ID:TC	-1.1	-1.2
RI:ID:TC	-1.0	-1.0
DF:ID:P	$+4.9$	$+5.0$
RI:ID:P	-2.6	-2.7

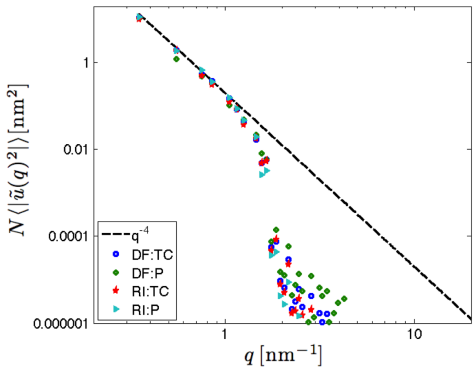

Figure S1: One-dimensional undulation spectrum obtained using a Hamming filter, calculated by averaging in q-space over circles of radii $q = \sqrt{q_x^2 + q_y^2}$. The filter transition at $q_0 = 1.15$ nm^{-1} is clear.

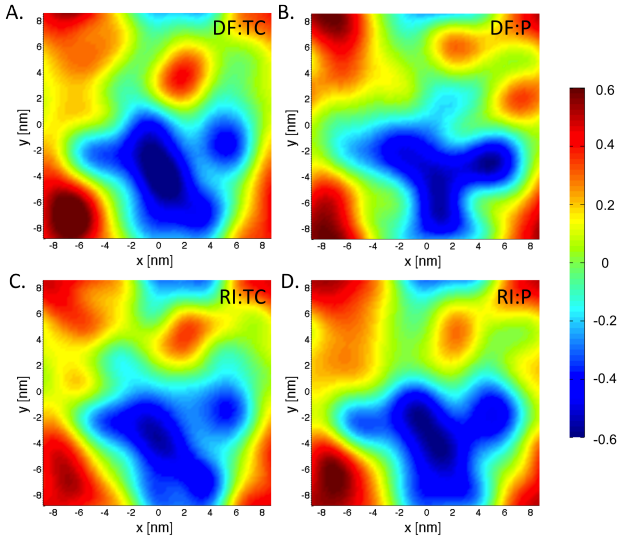

Figure S2: Single frame URS using the Hamming FIR filter with $q_0 = 1.15$ nm^{-1} for DF (A, B) and RI (C, D) methods using the TC (A, C) and P (B, D) atom definitions.

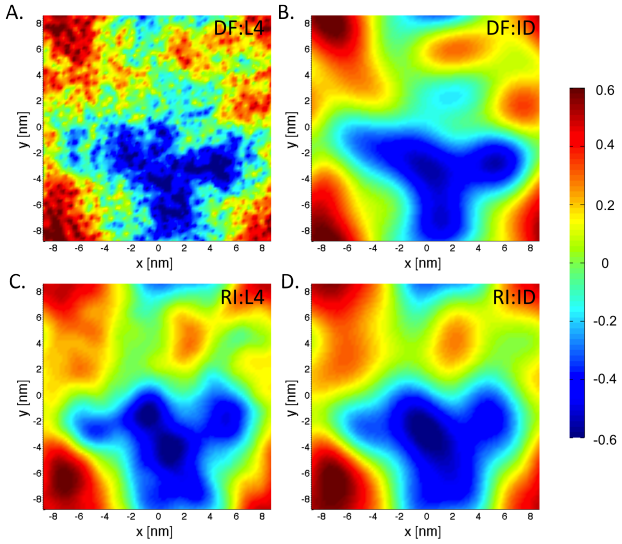

Figure S3: Single frame URS with $q_0 = 1.15$ nm^{-1} for the DF (A, B) and RI (C, D) methods using the phosphorus atom definition and filters L4 (A, C) and ID (B, D).

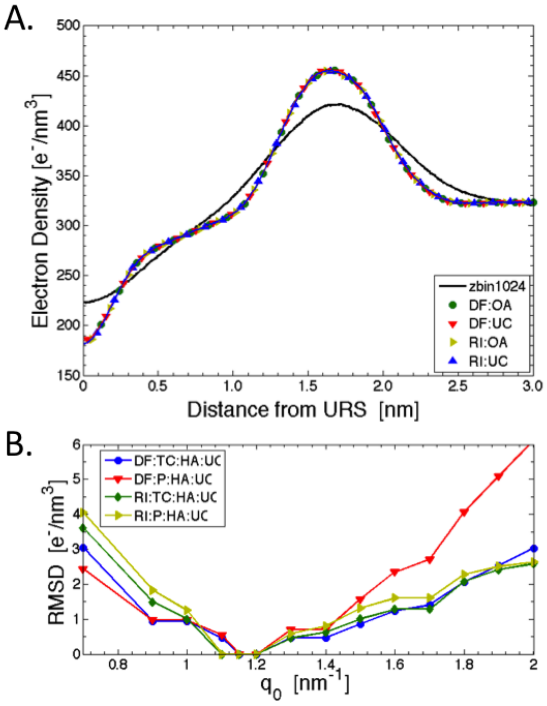

Figure S4: (A) EDP for Hamming filter, analogous to Fig. 5 of the main text (13). (B) RMSD measuring the difference between EDPs determined for a range of q_0 values compared to the EDP obtained at $q_0 = 1.15$ nm^{-1} using the Hamming filter for the methods indicated in the legend.

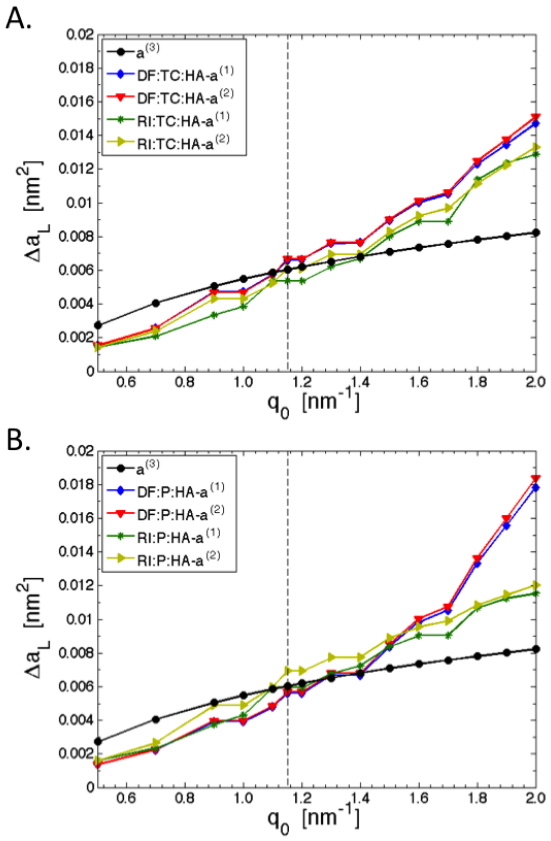

Figure S5: $\langle \Delta a_L \rangle$ versus q_0 for the DF and RI methods, for TC (A) and P (B) atom selections, using the Hamming filter. Results are reported for method a1, a2 and a3, respectively. The vertical dashed line shows $q_0 = 1.15$ nm^{-1}.

III. Undulation Reference Surfaces (URS)

This section reports detailed comparisons of the Root Mean Square Differences (RMSD) for undulation surfaces (defined as the average monolayer surface, see Fig. S6). The results, shown in Fig. S7 and Fig. S8, are sorted after method (DF or RI), atom selection (TC or P), filter treatment (ID, L4 or Hamming) and curvature correction (OA or UC).

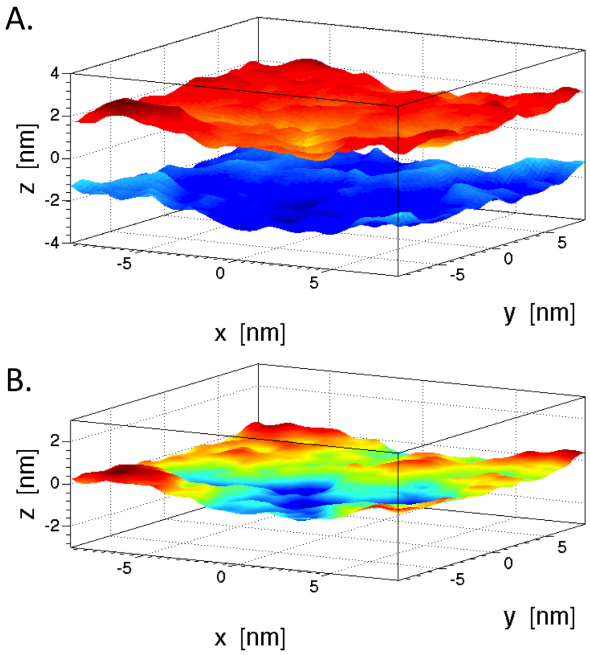

Figure S6: (A) Interpolated surfaces defining the top and bottom monolayers. (B) The undulation surface is defined as the average of the monolayer surfaces [Eq. 6 of the main text (13)].

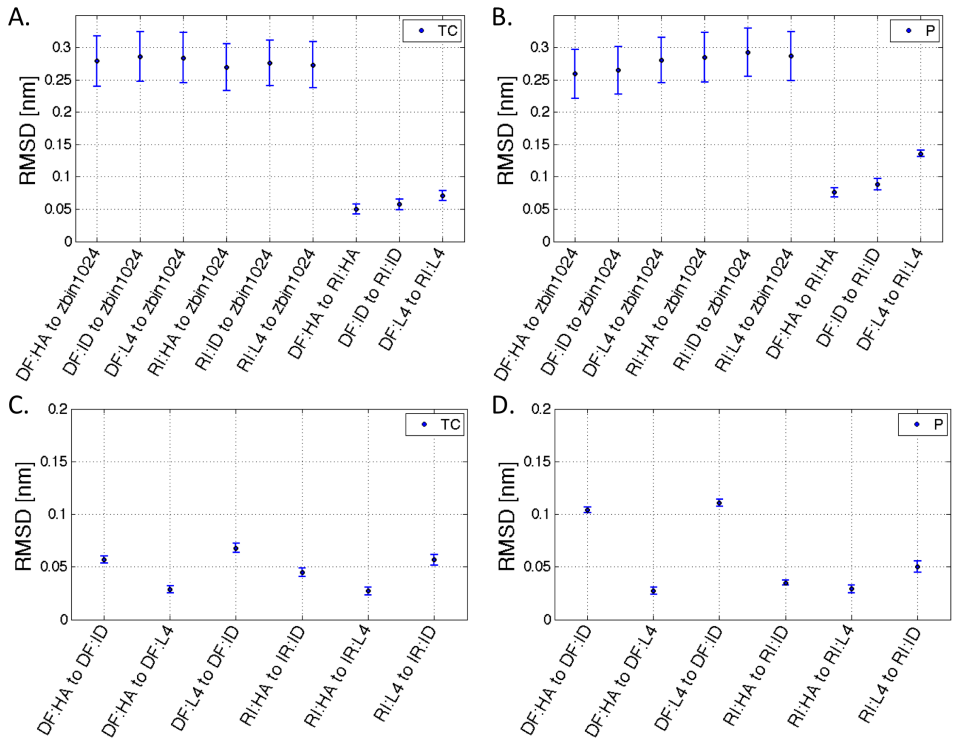

Figure S7: RMSD of differences between the URS obtained from the various methods. (A, B) Comparison of DF and RI methods. (C, D) Comparison of the HA, ID and L4 filter treatments.

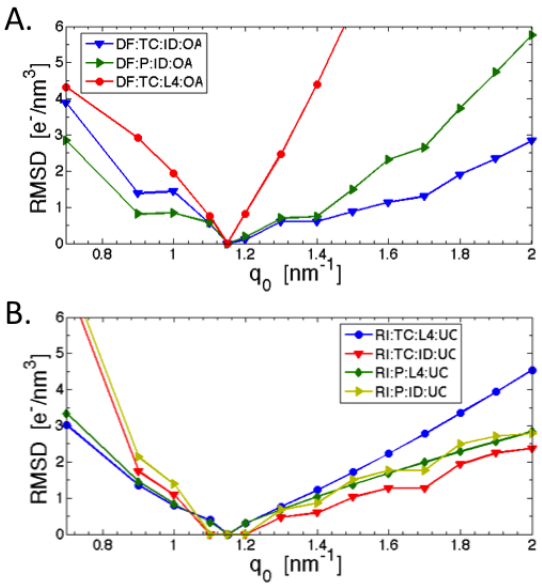

Figure S8: RMSD measuring the difference between EDPs determined for a range of q_0 values compared to the EDP obtained at $q_0 = 1.15$ nm^{-1} for (A) the DF:OA method and (B) the RI:UC method. The selection atom and filter are indicated in the legend.

IV. Electron Density Profiles (EDP)

This section reports on the accuracy of EDP calculated by different methods. Fig S9 compares RMSD, while Fig. S10 shows how the actually calculated EDP, and how their shapes are influenced by the method choice.

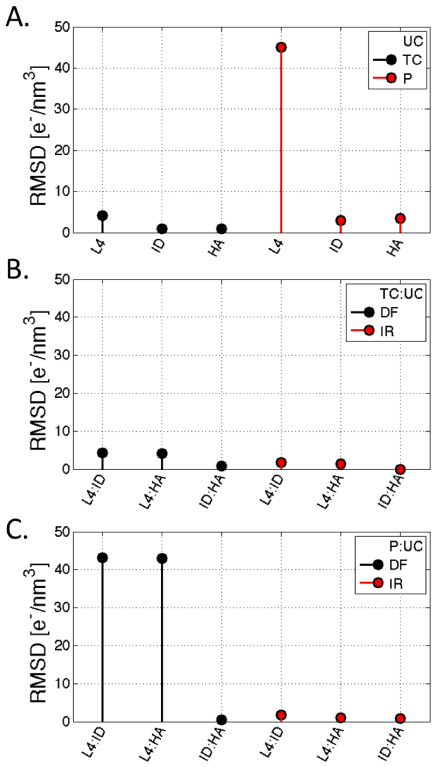

Figure S9: RMSD between EDP obtained by different methods using q_0 = 1.15 nm^{-1}. (A) Comparison of DF to RI method holding UC the same by filter (HA is Hamming) for TC (black) and P (red) selection atoms. (B) Comparison between filters for DF and RI methods using the TC selection atom. (C) Comparison between filters for DF and RI methods using the P selection atom.

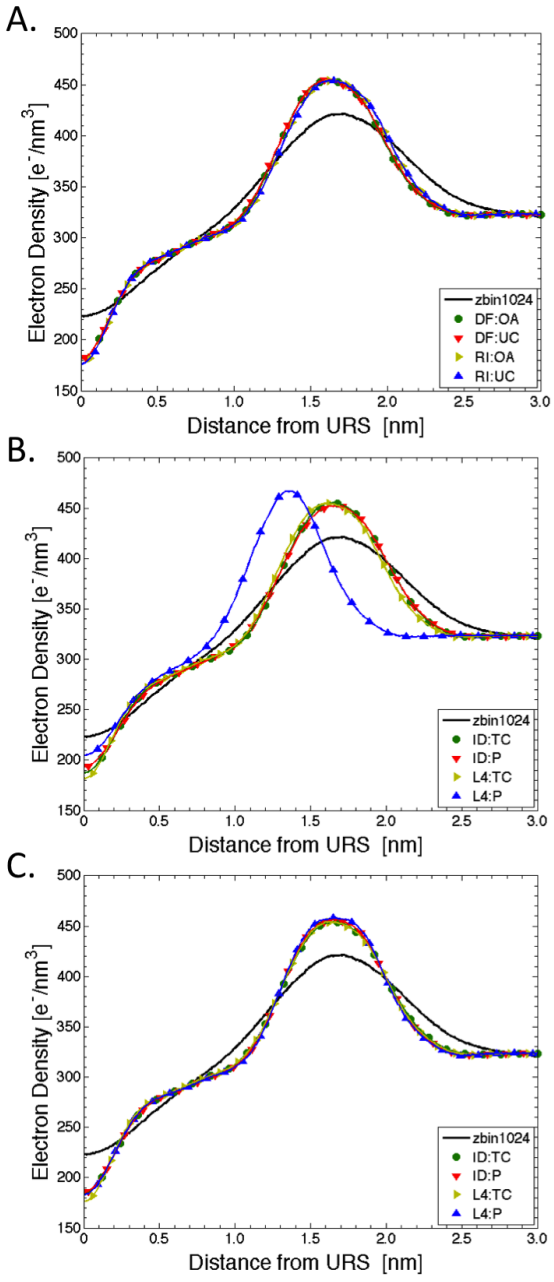

Figure S10: Comparison of EDP results for various methods. (A) is analogous to Fig. 5 of the main text (13), where DF to RI and OA to UC treatments are compared keeping TC:L4 the same instead of TC:ID in Fig. 5. (B) Using DF:UC, comparison of both ID and L4 filter treatment on TC and P atom selections. (C) Comparison of L4 to ID and TC to P keeping RI:UC the same. All panels include zbin1024 (black line) as reference.

V. Angular distributions

This section gives details regarding the local orientation approximation in the main text (13). The curvature correction is proportional to $\sin^2\theta$, making it small if θ is small. The θ-distributions are rather sensitive to the filter parameter q_0, for both DF and RI methods. This is shown in Fig. S11 for different q_0-values ($q_0 = 0.7, 1.15$, and $2.5\ \mathrm{nm}^{-1}$), comparing differences between URS method (DF and RI), atom choice (TC and P), as well as filter treatment (ID and L4). With $q_0 = 1.15\ \mathrm{nm}^{-1}$, the θ-distribution satisfies the small angle assumption of $\langle\theta\rangle \leqslant 10^\circ$ (14), but as q_0 increases beyond $2\ \mathrm{nm}^{-1}$ there is an increase in both the mean and width of the θ-distributions. This effect is more pronounced in the DF method due to the increasing contribution to the undulation intensity at large q from in-plane correlations (15). θ-values are calculated as absolute values.

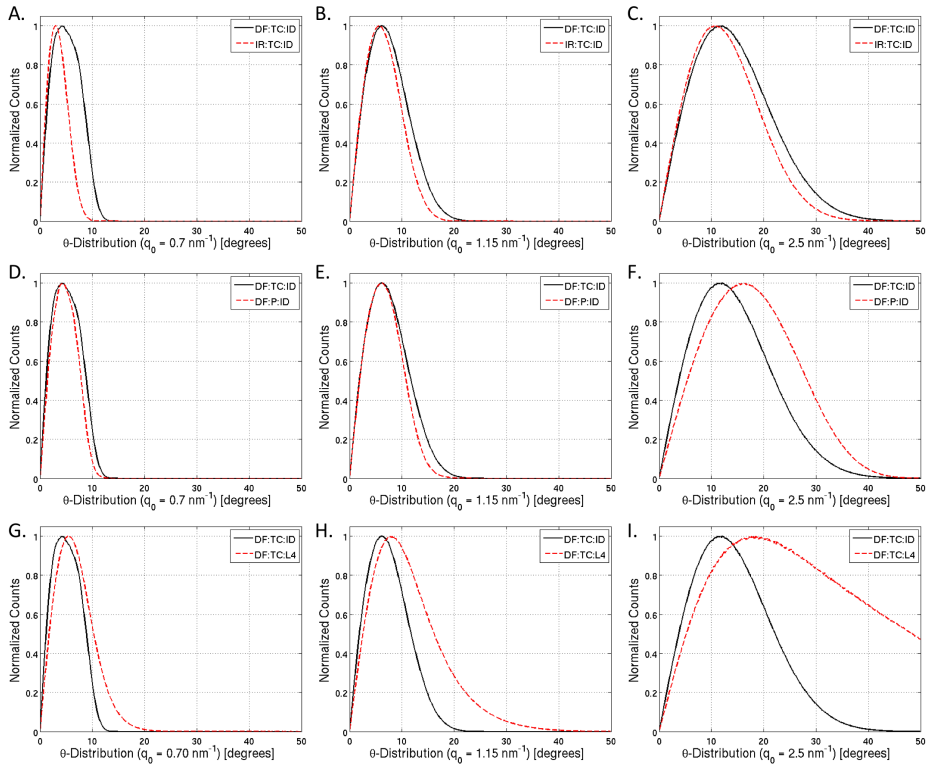

Figure S11: θ-distributions from a series of treatments for different values of the filter parameter, q_0 = 0.7(panels A,D,G), 1.15(panels B,E,H), and 2.5 nm^{-1}(panels C,F,I). Panels A–C compare DF to RI methods using the TC:ID treatment. Panels D–F compare the TC to P atom selections using the DF:ID treatment. Panels G–I compare ID to L4 filters for the DF:TC treatment.

VI. Areas

This section shows how the excess area calculations depend on the filter parameter q_0. Methods based on Fourier space calculations rely on the number of Fourier coefficients included in the surface reconstruction, which needs to be truncated to exclude wavelengths that correspond to molecular scales and below (see Fig. S12).

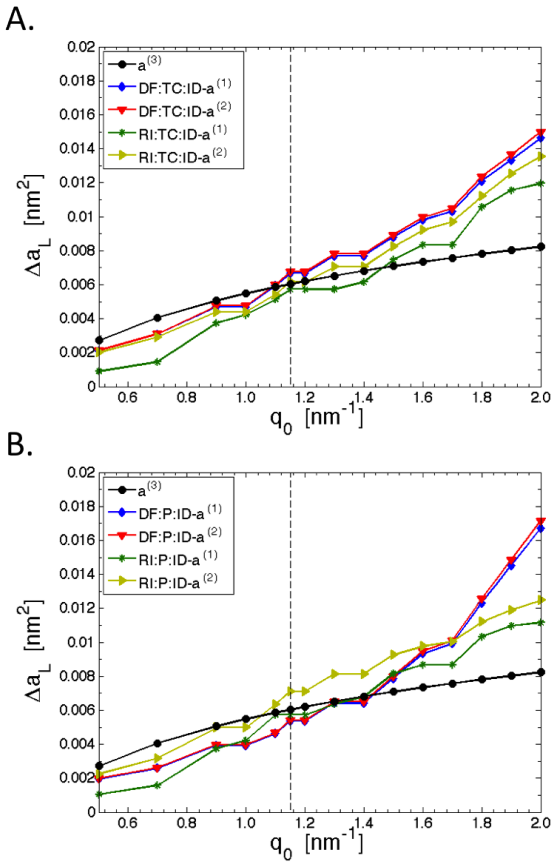

Figure S12: $\langle \Delta a_L \rangle$ versus q_0 for the DF and RI methods, for TC (A) and P (B) atom selections, using the ID filter. Results are reported for method a1, a2 and a3, respectively. The vertical dashed line shows $q_0 = 1.15$ nm^{-1}. When using a filter parameter $q_0 > 1.15$ nm^{-1}, the DF results are larger than the RI results, which is expected due to prefiltering in the RI method.

VII. Form factors

This section shows how the form factor, $F(q)$, which is the Fourier transform of the electron density, is influenced by the finite size effect. For system sizes exceeding 256 lipids, it is negligible (see Fig. S13).

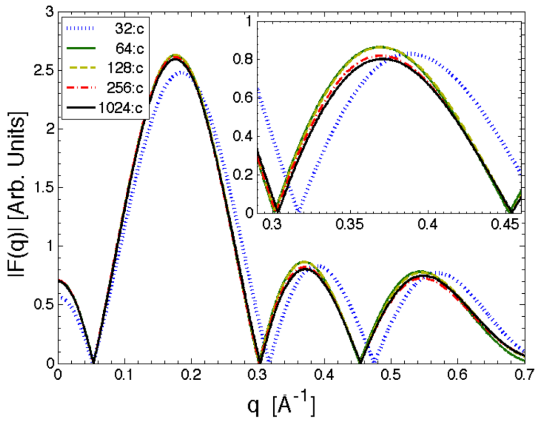

Figure S13: Comparison of DF:ID:TC:UC results for 32, 64, 128, 256 and 1024-lipid systems with $q_0 = 1.15$ nm^{-1}. Corrected form factor $F(q)$ for each system size with the inset focused on the second lobe, illustrating the finite size effects for smaller systems.

References

1. Pearson, R. H., and I. Pascher, 1979. The Molecular Structure of Lecithin Dihydrate. *Nature* 281:499–501.

2. Kuĉerka, N., Y. Liu, N. Chu, H. I. Petrache, S. Tristram-Nagle, and J. F. Nagle, 2005. Structure of Fully Hydrated Fluid Phase DMPC and DLPC Lipid Bilayers Using X-Ray Scattering from Oriented Multilamellar Arrays and from Unilamellar Vesicles. *Biophysical Journal* 88:2626–2637.

3. Berger, O., O. Edholm, and F. Jähnig, 1997. Molecular Dynamics Simulations of a Fluid Bilayer of Dipalmitoylphosphatidylcholine at Full Hydration, Constant Pressure, and Constant Temperature. *Biophysical Journal* 72:2002–2013.

4. Berendsen, H. J. C., J. P. M. Postma, W. F. van Gunsteren, and J. Hermans, 1981. Interaction Models for Water in Relation to Protein Hydration. *In* B. Pullman, editor, Intermolecular Forces, D. Reidel Publishing Company, Dordrecht, 331–342.

5. Hess, B., C. Kutzner, D. van der Spoel, and E. Lindahl, 2008. GROMACS 4: Algorithms for Highly Efficient, Load-Balanced, and Scalable Molecular Simulation. *J. Chem. Theory Comp.* 4:435–447.

6. Darden, T., D. York, and L. Pedersen, 1993. Particle Mesh Ewald: An $N \cdot \log(N)$ Method for Ewald Sums in Large Systems. *Journal of Chemical Physics* 98:10089–10092.

7. Essmann, U., L. Perera, M. L. Berkowitz, T. Darden, H. Lee, and L. G. Pedersen, 1995. A Smooth Particle Mesh Ewald Method. *Journal of Chemical Physics* 103:8577–8593.

8. Nosé, S., 1984. A Molecular Dynamics Method for Simulations in the Canonical Ensemble. *Molecular Physics* 52:255–268.

9. Hoover, W. G., 1985. Canonical Dynamics: Equilibrium Phase-Space Distributions. *Physical Review A* 31:1695–1697.

10. Parrinello, M., and A. Rahman, 1981. Polymorphic Transitions in Single Crystals: A New Molecular Dynamics Method. *Journal of Applied Physics* 52:7182–7190.

11. Nosé, S., and M. L. Klein, 1983. Constant Pressure Molecular Dynamics for Molecular Systems. *Molecular Physics* 50:1055–1076.

12. Oppenheim, A. V., and R. W. Schafer, 1989. Discrete-Time Signal Processing. *In* Discrete-Time Signal Processing, Prentice-Hall, 447–448.

13. Braun, A. R., E. G. Brandt, O. Edholm, J. F. Nagle, and J. N. Sachs, 2010. Electron Density Profiles and Areas from Molecular Dynamics Simulations of Undulating Lipid Bilayers. *Biophys. J.* submitted.

14. Nagle, J. F., and S. Tristram-Nagle, 2000. Structure of Lipid Bilayers. *Biochimica et Biophysica Acta (BBA) - Reviews on Biomembranes* 1469:159–195.

15. Brandt, E. G., A. R. Braun, J. N. Sachs, J. F. Nagle, and O. Edholm, 2010. Interpretation of Fluctuation Spectra in Simulations of Lipid Bilayers. *Biophysical Journal* submitted.